Please cite this article in press as: Verdaasdonk et al., Centromere Tethering Confines Chromosome Domains, Molecular Cell (2013), http://dx.doi.org/10.1016/j.molcel.2013.10.021

Molecular Cell
Article

Centromere Tethering Confines Chromosome Domains

Jolien Suzanne Verdaasdonk,[1] Paula Andrea Vasquez,[3] Raymond Mario Barry,[1] Timothy Barry,[1] Scott Goodwin,[1] M. Gregory Forest,[2] and Kerry Bloom[1,*]
[1]Department of Biology
[2]Department of Mathematics and Biomedical Engineering
University of North Carolina at Chapel Hill, Chapel Hill, NC 27599, USA
[3]Department of Mathematics, University of South Carolina, Columbia, SC 29208, USA
*Correspondence: kerry_bloom@unc.edu
http://dx.doi.org/10.1016/j.molcel.2013.10.021

SUMMARY

The organization of chromosomes into territories plays an important role in a wide range of cellular processes, including gene expression, transcription, and DNA repair. Current understanding has largely excluded the spatiotemporal dynamic fluctuations of the chromatin polymer. We combine in vivo chromatin motion analysis with mathematical modeling to elucidate the physical properties that underlie the formation and fluctuations of territories. Chromosome motion varies in predicted ways along the length of the chromosome, dependent on tethering at the centromere. Detachment of a tether upon inactivation of the centromere results in increased spatial mobility. A confined bead-spring chain tethered at both ends provides a mechanism to generate observed variations in local mobility as a function of distance from the tether. These predictions are realized in experimentally determined higher effective spring constants closer to the centromere. The dynamic fluctuations and territorial organization of chromosomes are, in part, dictated by tethering at the centromere.

INTRODUCTION

The foundations for our understanding of the physical organization of chromosomes originated in the work of Rabl and Boveri, who articulated a characteristic conformation in which centromeres (CENs) and telomeres are located at opposite sides of the nucleus, and this organization is maintained throughout the cell cycle (Boveri, 1909; Cremer and Cremer, 2010; Rabl, 1885; Spector, 2003). Chromosomes in budding yeast display a Rabl-like configuration in interphase (reviewed in Albert et al., 2012; Taddei and Gasser, 2012; Taddei et al., 2010; and Zimmer and Fabre, 2011). CENs are clustered and attached by microtubules to an unduplicated spindle pole body (SPB) (Dekker et al., 2002; Jin et al., 2000; O'Toole et al., 1999). Telomeres are located at the nuclear periphery in five to eight clusters in a manner dictated, at least in part, by chromosome arm length, with telomeres on arms of similar lengths clustering together (Bystricky et al., 2005; Dekker et al., 2002; Hediger et al., 2002; Jin et al., 2000; Schober et al., 2008). More recently, the characterization of the physical organization of chromatin within the nucleus has been described using chromosome conformation capture (3C) and high-throughput variants of this technique (de Wit and de Laat, 2012; Dekker et al., 2002; Dixon et al., 2012; Sanyal et al., 2011). Using a circular chromosome conformation capture (4C) followed by deep sequencing protocol, Duan et al. (2010) showed that budding yeast chromosomes occupy discrete areas of the nucleus around the tethered CENs. Population imaging of yeast nuclei has furthermore established the existence of chromosome territories (Berger et al., 2008) that are now perceived as a fundamental organizational feature of the nucleus (Austin and Bellini, 2010; Bickmore and van Steensel, 2013; Cremer and Cremer, 2010; Dixon et al., 2012; Hübner and Spector, 2010; Spector, 2003).

Various computational models have examined the formation of chromosomal territories and have shown that this organization can be explained by the inherent properties of a fluctuating polymer (Rosa and Everaers, 2008; Tjong et al., 2012; Wong et al., 2012). These models identify tethering, by simulating attachment at the CEN and telomere, and confinement, either by nuclear membrane or crowded polymer effects, as essential in modeling chromosome behavior and validate the starting point of our polymer model. By simulating the positioning of self-avoiding polymers, it has been suggested that entropic forces are sufficient to recapitulate the observed chromosomal territories (Cook and Marenduzzo, 2009; Finan et al., 2011). However, both the 3C variants and imaging to date have primarily examined the organization of nuclei in a whole population and lack information about the dynamics of chromatin organization within the cell nucleus.

We have quantified dynamic fluctuations along the length of the chromosome. The radius of confinement (R_c) is smaller at positions closer to the site of CEN attachment. We have examined the position-dependent fluctuations using a bead-spring polymer model of chromatin together with the biological constraints of nuclear confinement, crowding, and tethering. In vivo chromatin tethering and fluctuations underlie chromosome organization and dynamics. Thus, the organization of chromatin within the nucleus of interphase yeast cells is dictated by its confinement and proximity to an attachment point, and the dynamics can be approximated by the motion of an entropic spring.

RESULTS

Chromatin Confinement Varies along the Length of the Chromosome

We examined the in vivo dynamics of chromatin during interphase to determine the wild-type (WT) R_c at a discrete number

Please cite this article in press as: Verdaasdonk et al., Centromere Tethering Confines Chromosome Domains, Molecular Cell (2013), http://dx.doi.org/10.1016/j.molcel.2013.10.021

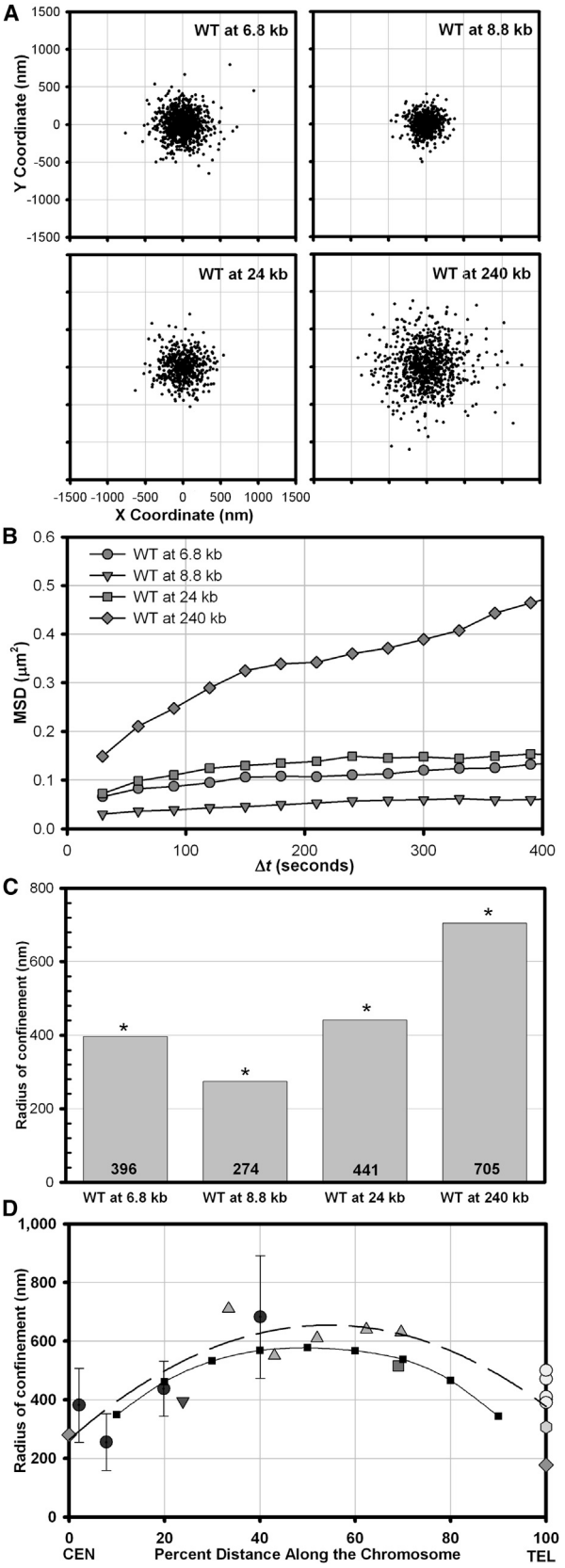

Figure 1. R_c of Chromatin Varies along the Length of the Chromosome

(A) Scatterplots illustrating variance in WT lacO/lacI-GFP spot position relative to spindle pole body.

(B) MSD curves of WT chromatin spot motion at various distances from the CEN.

(C) R_c values calculated using Equation 2 and whole population standard deviation values (Table 1). R_c values are all significantly different from each other (Levene's test, $p < 0.05$; Figure S2A). For comparison of R_c calculations using Equations 1 and 2, see Table S1 and Figure S1A.

(D) Experimental and literature R_c values plotted by percent distance from CEN (0%) and telomere (100%). The dashed line illustrates the general trend of reduced confinement at increasing distances from the attachment point. Dark circle, this work using individual cell variance, mean ± standard deviation (Table S1); light circle, Bystricky et al. (2005); square, Dion et al. (2012); hexagon, Hediger et al. (2002); diamond, Heun et al. (2001); inverted triangle, Miné-Hattab and Rothstein (2012); triangle, Neumann et al. (2012); black squares—our tethered bead-spring model (see Results).

of sites along the length of the chromosome. To do this, we both tracked a GFP-labeled chromatin array (lacO/lacI-GFP) at 6.8 kb (ChrXV), 8.8 kb (ChrIII), 24 kb (ChrIII), and 240 kb (ChrII) from the CEN and relative to the unduplicated SPB (Spc29-RFP) over 10 min at 30 s intervals and measured subpixel localization by Gaussian fitting over time. The 240 kb lacO array is positioned roughly midway between the CEN and telomere. The distribution of spot positions shows that arrays integrated further from the CEN can explore a larger space as compared to those more proximal to the point of attachment (Figure 1A). In order to quantify the subnuclear confinement observed, we use two methods to calculate R_c. From the plateau of the mean square displacement (MSD) curve (Figure 1B), 2D MSD gives (Neumann et al., 2012; Experimental Procedures)

$$R_c = \frac{5}{4} * \sqrt{MSD_{plateau}}. \qquad \text{(Equation 1)}$$

From the standard deviation of spot positions, σ, and the average squared deviation from the mean position, $\langle \Delta r_0^2 \rangle$, we applied the equipartition theorem to calculate R_c from random chromatin motion (Scheffold et al., 2010; Uhlenbeck and Ornstein, 1930; Experimental Procedures) to get

$$R_c = \frac{5}{4} * \sqrt{2\sigma^2 + \langle \Delta r_0^2 \rangle}. \qquad \text{(Equation 2)}$$

Equations 1 and 2 are not statistically different for positions close to the tether (Student's t test, $p < 0.05$; Table S1 and Figure S1A available online). The plateau value from MSD is more variable, as it is based on long lag times between spot measurements and uses a fraction of the total data. Therefore, we use Equation 2 and the standard deviation obtained with the entire data set to calculate R_c throughout this work.

The R_c is largest for the chromatin spot furthest from the CEN at 240 kb (705 nm, 43 cells) and smallest for spots proximal to the CEN at 8.8 kb (274 nm, 40 cells) and 6.8 kb (396 nm, 54 cells), suggesting that the attachment at the CEN functions to constrain chromatin movement (Figure 1C; Table 1). Statistical comparison revealed that R_c values of chromatin spots at these four distances from the CEN are all statistically different from each other (Levene's test, $p < 0.05$; Figure S2A; Levene, 1960). This pattern is a generalized feature of chromosomes in yeast (Figure 1D;

Table 1. Summary of R_c and k_s Measurements from Population Variance

LacO Array Distance from Centromere	Relevant Genotype/Conditions	Sample Size	Radius of Confinement (R_c) (nm) = $5/4 * \sqrt{2\sigma^2 + \langle \Delta r_0^2 \rangle}$ (Population σ)	Effective Spring Constant (k_s) (pN/nm) = $k_B T/\sigma^2$ (Population σ)	Fold over Entropic Spring
240 kb	WT (Chr II)	43	705	5.1×10^{-5}	33×
24 kb	WT (Chr III)	25	441	1.3×10^{-4}	9×
8.8 kb	WT (Chr III)	40	274	3.4×10^{-4}	8×
6.8 kb	WT (Chr XV)	54	396	1.6×10^{-4}	3×
8.8 kb	Gal-CEN on galactose	23	745	4.6×10^{-5}	1×
240 kb	WT, 37C	16	691	5.4×10^{-5}	35×
240 kb	*mcd1-1*	25	892	3.2×10^{-5}	21×
240 kb	*mcd1-1*, 37C	33	958	2.8×10^{-5}	18×
6.8 kb	Gal-H3 on glucose	55	319	2.5×10^{-4}	5×
6.8 kb	WT, α factor	43	380	1.8×10^{-4}	3×

Bystricky et al., 2005; Dion et al., 2012; Hediger et al., 2002; Heun et al., 2001; Miné-Hattab and Rothstein, 2012; Neumann et al., 2012).

Chromatin Dynamics in Interphase Are Dictated by Tethering

In order to determine whether the R_c observed adjacent to the CEN is dictated by microtubule attachment or an inherent property of the pericentric chromatin, we tracked chromatin motion in cells in which the CEN has been detached through its conditional inactivation (Hill and Bloom, 1987; Figure 2A). The insertion of the galactose (GAL) promoter adjacent to the CEN allows the CEN to function normally when grown on glucose and inactivated when on GAL. Detachment upon CEN inactivation results in a dramatic increase in the R_c at 8.8 kb from the CEN from 274 nm (40 cells) to 745 nm (23 cells) (Figure 2B; Table 1), demonstrating that this chromatin region can explore a larger space when no longer attached to the SPB. It is unlikely that this increased motion is the result of transcription induced by the GAL promoter, as these loci have previously been shown to be confined at the periphery (Brickner et al., 2007; Drubin et al., 2006). Chromatin confinement at maximal distance from attachment (lacO at 240 kb) and detached upon CEN inactivation (Gal-CEN at 8.8 kb on GAL) is not statistically different (Levene's test, $p < 0.05$). LacO at 8.8 kb is statistically different from both lacO at 240 kb and Gal-CEN at 8.8 kb (Levene's test, $p < 0.05$; Figure S2A). This indicates that the confinement of the 8.8 kb chromatin spot is due to attachment at the CEN and not an inherent property of this region of chromatin. The tethering of chromatin is a universal organizational feature and has important implications for the temporal and spatial fluctuations of chromosomes.

The Chromatin Polymer Behaves like an Elastic Filament during Interphase

Throughout our in vivo time-lapse movies, we observed transient spot expansion of lacO/lacI-GFP-labeled chromatin arrays in G1 (Figures 3A–3D). Chromatin arrays stretch during mitosis, presumably as a consequence of microtubule pulling force (Stephens et al., 2011; Stephens et al., 2013). Spot expansion during G1 could be the result of microtubule dynamics (as chromosomes remain attached at their CENs) and/or the inherent spring properties of the polymer. We defined a change in the lacO arrays by measuring the ratio of the axes of a 2D Gaussian fit to the GFP signal. A spot was defined as expanded when the long axis was at least 1.5 times larger than the smaller axis. The lacO/lacI-GFP array at 240 kb from the CEN was found to exhibit expansion in 16% of time points imaged (141/879 planes), and the CEN-proximal (6.8 kb from the CEN) chromatin spot exhibited expansion in 10% of time points imaged (109/1105 planes) (Figures 3A and 3C). Examples of lacO/lacI-GFP dynamics in live cells are plotted in Figures 3B (240 kb) and 3D (6.8 kb). These transient extensions are of relatively short duration, lasting less than a few minutes. On average, the chromatin spot at 240 kb from the CEN had higher mean and median ratios than the 6.8 kb chromatin spot (Figure S3A). We observed recoiling of these chromatin spots, indicating that the chromatin was behaving like an elastic filament. The spot expansion and contraction are variable and often deformed (see variability of expansion shapes, Figures 3A and 3C); thus, chromatin motion in interphase shows no coherent properties. The random trajectory of energy-dependent processes acting on the chromatin validates the rationale for using the equipartition theorem to estimate confinement (Equation 2). In addition to aspect ratio, we examined variance in distance between two loci (lacO/lacI-GFP and tetO/tetR-CFP) adjacent to the CEN of chromosome XI to assess chromatin polymer elasticity (Figure S3B). We find that both aspect ratio and variance in spot distances reveal the elastic nature of the chromatin.

Modeling the Chromatin Spring as a Doubly Tethered, Confined Bead-Spring Chain with Excluded Volume Interactions Can Recapitulate Experimental Dynamics

In order to model the dynamic behavior and gain insight into chromosome organization, we construct a 2D bead-spring model of a doubly tethered polymer chain using Brownian beads connected by linear springs (Doi and Edwards, 1986; Experimental Procedures; Figure 4A). The chain is tethered at both ends to simulate the CEN and telomere attachments, confined within a 1 μm circle (the nucleus) and subject to excluded volume interactions. The bead-spring chain has a persistence length (L_p)

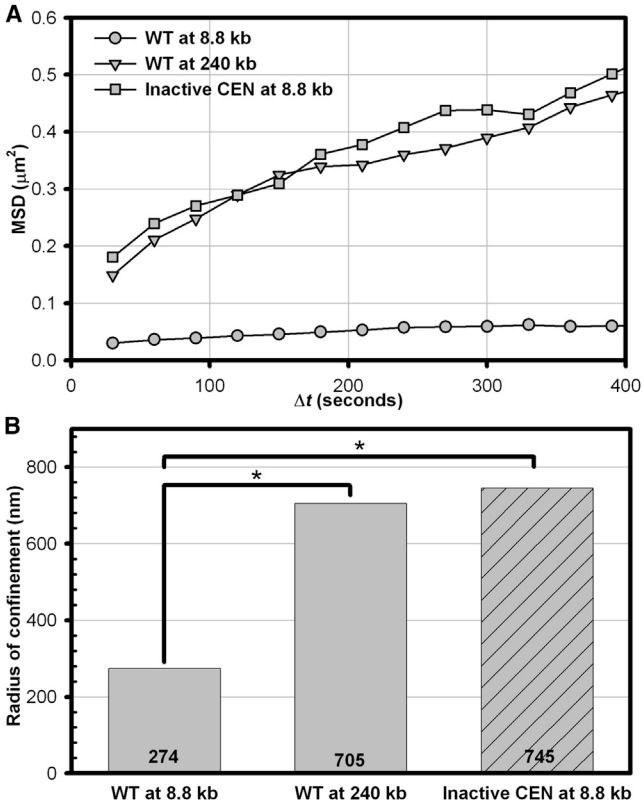

Figure 2. R_c Is Dictated by the Attachment at the Centromere

(A) MSD analysis of cells in which the CEN has been detached through its conditional inactivation (Gal-CEN on GAL) revealed reduced confinement of a lacO/lacI-GFP-labeled chromatin spot 8.8 kb from the CEN as compared to WT at 8.8 kb.

(B) Bar graph of R_c values (Equation 2). Statistical comparison shows WT at 8.8 kb and inactive CEN at 8.8 kb to be statistically significantly different from each other, whereas WT at 240 kb and inactive CEN at 8.8 kb are not statistically significantly different from each other (Levene's test, $p < 0.05$; Figure S2A).

of 50 nm, corresponding to the known value for DNA. The L_p is defined as the distance over which the correlation of the direction of the two ends is lost, and longer L_p implies stiffer polymer chains (Bloom, 2008). We modeled one arm of a chromosome as 100 beads connected by 99 springs with a packing density in between that of the 11 nm and 30 nm fibers (Experimental Procedures, "Defining Model Variables"). R_c values along the chain compare to experimental values and are smaller at positions closer to the tether point (Figure 1D, black squares). The varying radii of confinement observed in vivo can be recapitulated by a doubly tethered bead-spring model. We note that in the absence of tethering, all positions within the chain will have the same radius of the circle (R_c) (Rosa and Everaers, 2008). Thus, tethering results in variations of R_c with respect to the distance from the CEN. We found that the qualitative behavior of R_c along the chain remains unchanged when the radius of the nucleus is changed; however, the magnitude of R_c decreases with the radius.

While the bead-spring chain consists of identical springs between each pair of beads, the effects of tethering, geometric confinement, and excluded volume interactions result in distinct statistical fluctuations of each bead (lacO/lacI-GFP position experimentally) along the chain. This leads to a position-dependent effective spring constant (k_s), as seen by a particular bead relative to the tether points and measured based on that bead's fluctuations as described below. The tendency of the spring to adopt a random coil can be represented in terms of a spring constant that reflects the spring stiffness (Bloom, 2008). The effective spring constant (k_s) for bead *i* in our model is given by

$$k_{s,i} = 3k_BT\left(\frac{C_r}{2L_p \times L_c}\right)\left(\frac{1}{p(1-p)}\right), \qquad \text{(Equation 3)}$$

where k_B is the Boltzmann constant, T is temperature (kelvin), L_p is persistence length, L_c is contour length, C_r is ratio of compaction, and p is the percentage of the chain from the CEN (Experimental Procedures). From the displacement of the beads in our model, we estimate k_s as a function of position along the chain (Figure 4B). This observation reveals the limitation in deducing a spring constant from measurements of a single spot along the chain. The k_s is smaller for beads that "explore" a larger space, and so the k_s will be highest (stiffest) for positions close to the tether point and softest in the middle of the chain. Thus, tethering of an otherwise homogeneous bead-spring chain results in a gradient of k_s along the chain and introduces variations in local mobility.

The Effective Spring Constant along the Entropic Chromatin Spring Can Be Measured In Vivo

We calculate an effective k_s from our in vivo time-lapse data using two methods (Experimental Procedures). Using the MSD plateau value and the average squared deviation of each step from the mean position $\langle \Delta r_0^2 \rangle$, we calculated (Bruno et al., 2011; Kamiti and van de Ven, 1996)

$$k_s = \frac{2k_BT}{\langle MSD_{plateau} \rangle - \langle \Delta r_0^2 \rangle}. \qquad \text{(Equation 4)}$$

Using the equipartition theorem, we measured the standard deviation (σ) of each step from the mean position to calculate (Scheffold et al., 2010)

$$k_s = \frac{k_BT}{\sigma^2}. \qquad \text{(Equation 5)}$$

Similar to R_c, k_s values were calculated using both methods for lacO at 6.8 kb, 8.8 kb, 24 kb, and 240 kb from the CEN (Figure S1B; Table S1). We found significant agreement between the two methods; a Student's t test comparing k_s values calculated using Equations 4 and 5 for individual cells showed no statistical differences between the two methods (Student's t test, $p < 0.05$). As previously described for R_c calculations, the plateau method uses a fraction of the total data set. Thus we use the equipartition method (Equation 5) and the standard deviation obtained from the entire data set for remaining calculations.

From Equation 5, we see that in general stiffness varies inversely with position variance, meaning that for loci exhibiting smaller variance, the chromatin will have a higher effective spring constant (Figure 1A). As predicted by our model, k_s was found to vary with distance from the tether point and appeared stiffer at

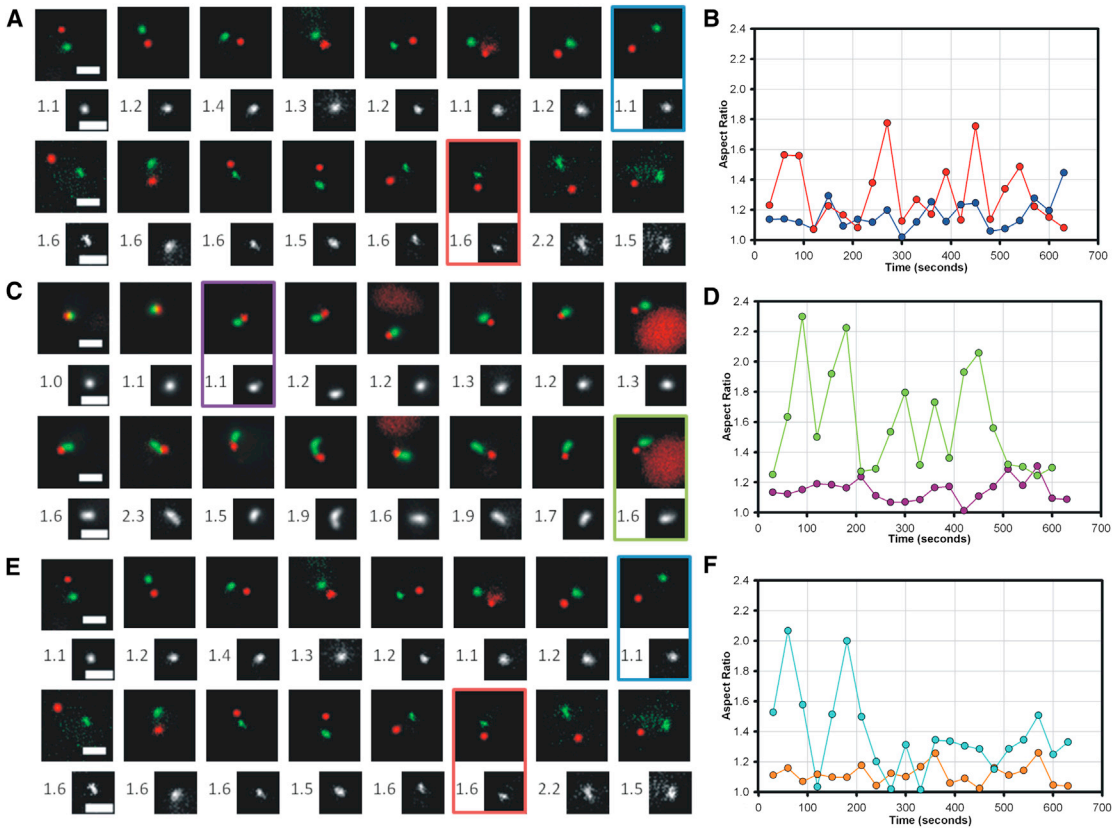

Figure 3. Interphase Chromatin Is Dynamic

(A) Example images of lacO/lacI-GFP at 240 kb from the CEN with aspect ratios less than and greater than 1.5 (compacted and decompacted). Measured aspect ratios are shown.

(B) Graph of aspect ratio change over time for two cells, colors corresponding to outlined images in (A).

(C and D) (C) Example images of lacO/lacI-GFP at 6.8 kb and (D) graphs of aspect ratio changes for two examples. WT cells exhibit transient expansion and recompaction of chromatin arrays along random and occasionally nonlinear trajectories.

(E) Example images of lacO/lacI-GFP at 6.8 kb in Gal-H3 cells in which nucleosomes have been depleted and (F) graphs of aspect ratio changes over time. Aspect ratio values of lacO/lacI-GFP signal = large axis/small axis. Scale bar = 1 μm. Time-lapse images were taken every 30 s. Color images: lacO/lacI-GFP is in green; spindle pole body (Spc29-RFP) is in red. Black and white images show lacO/lacI-GFP with corresponding aspect ratios alongside.

points closer to the site of attachment, and regions within the pericentromere domain exhibit a variation in stiffness (lacO at 6.8 kb, 1.6×10^{-4} pN/nm; 8.8 kb, 3.4×10^{-4} pN/nm; 24 kb, 1.3×10^{-4} pN/nm; 240 kb, 5.1×10^{-5} pN/nm) (Figure 4D; Table 1). Statistical comparison of population variances showed these to all of these to be significantly different from each other (Levene's test, $p < 0.05$; Figure S2A). Application of equipartition methods to our data represents a starting point to quantify these dynamics, and further work will refine the applied mathematics to more closely match in vivo conditions.

Upon detachment from the CEN (Gal-CEN), the k_s for a chromatin spot 8.8 kb from the CEN is reduced as compared to WT at 8.8 kb and appears softer and approaches the value of the chromatin arm at 240 kb (Gal-CEN at 8.8 kb, 4.6×10^{-5} pN/nm, Figure 4D; Table 1). Statistical comparison found Gal-CEN at 8.8 kb to be significantly different from WT at 8.8 kb, but not significantly different from WT at 240 kb (Levene's test, $p < 0.05$; Figure S2A). This confirms the prediction that the apparent properties of the chromatin polymer are dictated by the attachment to a tether point like the CEN. The gradient of k_s is the result of tethering and provides a mechanism to build variations in local mobility along the chromatin chain. This implies a role for tethering in the differential regulation of various regions of chromatin by altering polymer properties such as dynamics and stiffness. By attaching or detaching chromatin from a tether, the cell can efficiently alter the stiffness, as well as the range of motion, of the chromatin.

Cohesin Contributes to Local Clamping of Chromatin

A major source of chromatin organization is the structural maintenance of chromosomes protein complex cohesin. While the role of cohesin in holding sister chromatids together in mitosis is well established, it is becoming increasingly evident that cohesin also serves a vital role in interphase chromatin gene regulation through looping (as reviewed in Haering and Jessberger, 2012; Seitan and Merkenschlager, 2012; and Sofueva and Hadjur, 2012). Given the regulatory role for cohesin looping, we predict a role for cohesin in the organization of chromatin into territories and maintaining chromatin dynamics during interphase.

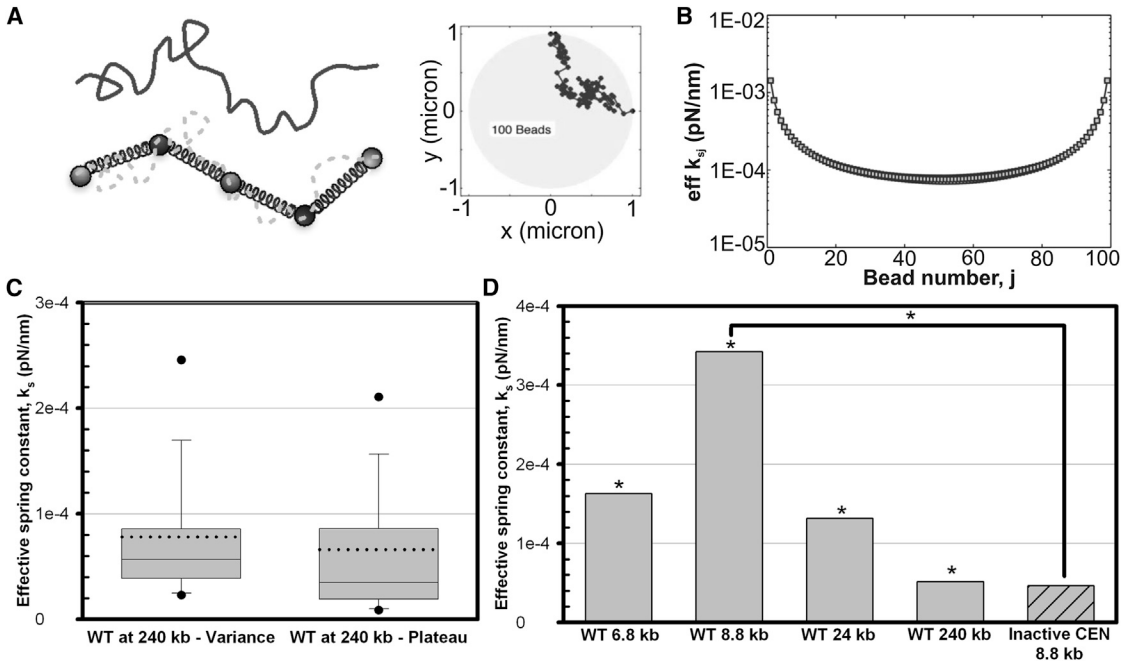

Figure 4. Modeling Interphase Chromatin Dynamics as a Doubly Tethered Bead-Spring Polymer Chain

(A) The chromatin polymer (solid line) can be modeled as a bead-spring polymer chain (dotted line indicates original chromatin polymer chain). Diagram of a bead-spring chain composed of 100 beads tethered at both ends and confined within a circle of radius 1 μm.

(B) The effective spring constant (k_s; Equation 3) is highest (stiffest) for beads closest to the tether points (beads 0 and 100) and softest in the middle of the chain (at bead 50).

(C) Measurement of k_s from in vivo dynamic MSD data at various positions from the CEN. We compared k_s calculated using the MSD plateau value (right, Equation 4) or the variance of the distribution of spot positions (left, Equation 5) and found no significant difference in WT cells at 240 kb from the CEN (Student's t test, $p > 0.05$; Table S1). Solid lines indicate median; dotted lines indicate mean. Black dots above and below indicate 95%/5% percentiles of the data distribution. (For comparisons at 24 kb, 8.8 kb, and 6.8 kb from the CEN, see Figure S1B.)

(D) K_s values calculated using the variance of the distribution of spot positions of the whole population (Equation 5; Table 1). Consistent with the doubly tethered bead-spring polymer chain model, the chromatin exhibited a higher k_s (stiffer spring) closer to the tether point (at 6.8 kb and 8.8 kb from the CEN) and lower k_s (softer spring) in the middle of the chromosome (at 240 kb from the CEN). The high k_s observed close to the CEN is due to attachment at the CEN and is not an inherent property of this region of chromatin. When the CEN is detached through its conditional inactivation (Inactive CEN), the k_s at 8.8 kb from the CEN is reduced. Statistical comparisons at four WT positions are statistically significantly different from each other. Upon conditional CEN inactivation (Inactive CEN), the measured k_s at 8.8 kb is significantly softer from the measured k_s for WT at 8.8 kb (Levene's test, $p < 0.05$; Figure S2A).

We examined R_c and effective k_s of the lacO/lacI-GFP array at 240 kb from the CEN in WT and *mcd1-1* cells at permissive (24°C) and restrictive (37°C) temperatures (Figure 5A). The R_c is increased in *mcd1-1* cells at restrictive temperature as compared to *mcd1-1* at permissive or WT (WT at 24°C, 705 nm, 43 cells; WT at 37°C, 691 nm, 16 cells; *mcd1-1* at 24°C, 892 nm, 25 cells; *mcd1-1* at 37°C, 958 nm, 33 cells; Figure 5B; Table 1). This does not result from increased temperature, as WT cells at 37°C do not show a similar increase in R_c. In addition, k_s is decreased in *mcd1-1* cells at restrictive temperature as compared to WT at 37°C, suggesting that the chromatin spring is softer upon the loss of cohesin (WT at 24°C, 5.1×10^{-5} pN/nm; WT at 37°C, 5.4×10^{-5} pN/nm; *mcd1-1* at 24°C, 3.2×10^{-5} pN/nm; *mcd1-1* at 37°C, 2.8×10^{-5} pN/nm; Figure 5C; Table 1). Statistical comparison of population variances found no statistical difference between WT at 24°C and WT at 37°C, whereas *mcd1-1* at 24°C and *mcd1-1* at 37°C were both statistically different from WT and from each other (Levene's test, $p <$ 0.05; Figure S2B).

To model the reduction of cohesin and predict its physiological role, we have examined the dynamics of chains composed of more beads (from N = 100 to N = 150 at a constant L_p = 50 nm) (Experimental Procedures; Figure 5D). We reason that chromatin in loops will not contribute to the effective chromatin length, and upon loss of cohesin and release of loops, additional chromatin will lengthen the chain. In the model this reduces the compaction ratio, and at the same L_p, which increases the number of beads (number of beads = $(L_c/C_r)/2L_p$)). The model predicts that upon an increase in effective chromatin length (i.e., more beads in the chain), the R_c for any given point should increase and the k_s will decrease (Figure 5D), consistent with the experimental results.

Nucleosome Depletion Results in a Stiffer Chromatin Fiber

We hypothesize that changes to nucleosome density would have important effects on chromatin fluctuations. We tested the effects of changing chromatin packaging on dynamics by

measuring R_c and effective k_s in cells with reduced nucleosome occupancy. We measured the MSD dynamics of a chromatin spot 6.8 kb from the CEN in a strain depleted of histone H3 that results in a 2-fold reduction of nucleosome density (Bouck and Bloom, 2007; Figure 5E). The R_c was statistically significantly reduced from 396 nm (54 cells) to 319 nm (55 cells) (Levene's test, $p < 0.05$; Figure 5F; Table 1; Figure S2C). The k_s was statistically significantly increased, becoming slightly stiffer from 1.6×10^{-4} pN/nm to 2.5×10^{-4} pN/nm (Levene's test, $p < 0.05$; Figure 5G; Table 1). These effects were not due to α factor arrest, which was not found to significantly alter R_c or k_s (Figures 5E–5G; Table 1; Figure S2C). From these data, we conclude that nucleosomal packaging is an important factor in dictating the spatiotemporal organization and fluctuations of the chromatin polymer.

The reduced nucleosomal density in H3-depleted cells will increase the fraction of naked DNA from ~20 bp/nucleosome (based on linker length) to ~160 bp/2 nucleosomes, or ~80 bp/nucleosome (based on loss of half the number of nucleosomes). This will disproportionally alter the physical properties of the chromatin. Unlike cohesin depletion in which the fraction of naked DNA is constant, we model the increase in naked DNA as a decrease in L_p. Bystricky et al. have reported that DNA has a substantially shorter L_p than chromatin (Bystricky et al., 2004). The model predicts that by decreasing L_p, R_c for any given bead decreases (data not shown) and its k_s increases (Figure 5H).

The lacO/lacI-GFP spot morphology provides a quantitative assay for chromatin elasticity. The CEN-proximal (6.8 kb) chromatin spot exhibited expansion in 10% of time points imaged (WT, 109/1,105 time points) and reduced to 3% upon histone H3 depletion (36/1,148 time points) (Figure 3E). The stiffer k_s at 6.8 kb from the CEN observed in nucleosome-depleted cells would predict that fewer cells would exhibit expansion (aspect ratio > 1.5) of the CEN-proximal lacO/lacI-GFP array, since it would take more energy to extend the entropic spring. Reduced nucleosome density would result in unwrapping of the DNA from nucleosomes and a general increase in spot size. We examined the morphology of the CEN-proximal lacO/lacI-GFP-labeled chromatin spot and observed an average increase in spot size for both compacted (aspect ratio < 1.5) and decompacted (aspect ratio > 1.5) spots (Figure S4). We have directly assessed the dynamic physical consequences of changing the histone compaction and measured a higher effective k_s for a chromatin spot 6.8 kb from the CEN in nucleosome-depleted cells. Nucleosomal density, and therefore L_p and linker length, are important factors in determining the physical properties of the entopic chromatin spring.

Dynamic Fluctuations Underlie Chromosome Territories

Chromosome territories within a population of cells can be visualized in chromosome interaction maps. In order to examine if our tethered bead-spring model describes the formation of chromosome territories within the dynamic nucleus, we generated interaction maps of four tethered chains within a circle. We examined the bead position distributions in our polymer model (Figures 6A and 6B) and plotted the average normalized bead separation (Figures 6C and 6D). Telomeric attachment in budding yeast is known to occur in five to eight foci and in Rabl-like configuration (Bystricky et al., 2005); therefore, we considered either five attachment points analogous to one CEN position and four discrete telomere attachment points (Figure 6A) or three attachment points (one CEN position and two telomere points) (Figure 6B). The combination of excluded volume interactions and shorter distance between tether points results in a more uniform heatmap distribution (Figures 6A and 6C, chains 1 and 4; Figures 6B and 6D, chains 3 and 4). When the tethers are further apart and the chain is able to explore a larger space, beads along the middle of the chain rarely come into contact (blue on the heatmaps), and excluded volume interactions dominate over confinement. The chromosome interaction maps reveal a potential regulatory mechanism in the position of the telomere attachment site. The tethered regions of a single chain, while sampled infrequently, provide the ability for disparate chains to physically interact with one another. This provides a mechanism for distinct chains within the nucleus to share genetic information, while satisfying the territories of individual chains.

DISCUSSION

In Vivo Measurements of Fundamental Chromosome Properties—R_c and Effective k_s

Through a combination of experimental observation and mathematical modeling we have shown that interphase chromatin fluctuations are mainly governed by attachment at the CEN and telomere. Loss of attachment allowed CEN-proximal chromatin to soften (lower effective k_s) and explore more space (higher R_c), behaving like a region out on the chromosome arm. By formulating a 2D bead-spring model based on simple polymer physics, we captured the observed k_s along the length of the chromosome. To capture relevant experimental features the model requires the following: (1) tethering at both ends, (2) confinement within a domain, and (3) excluded volume interactions between beads.

In order to determine the effect of polymer length on chromosome fluctuations, we examined dynamics in cohesin-depleted cells. Loss of cohesin effectively lengthens the chromosome, since less of the total length is confined in loops. This led to softening of the chromatin fiber at 240 kb from the CEN and allowed this region to explore a larger space. Thus, the overall length of the chromosome is an important factor in determining its spatiotemporal fluctuations, consistent with polymer theory (Equation 6) in which the spring constant is inversely related to number of segments (N). In addition to chromosome length, the L_p of the polymer is predicted to play an important role in chromosome fluctuations. As L_p is decreased, the spring constant will increase by virtue of the increase in number of entropic states, and the polymer will occupy a smaller radius of gyration (Bloom, 2008). In order to test this, we hypothesized that reduced nucleosome occupancy results in a lower average L_p (DNA L_p = 50 nm versus chromatin L_p = 170–220 nm [Bystricky et al., 2004]). Consistent with the theory, we observed stiffening of the CEN-proximal chromatin (higher k_s) and smaller R_c in nucleosome-depleted cells.

Please cite this article in press as: Verdaasdonk et al., Centromere Tethering Confines Chromosome Domains, Molecular Cell (2013), http://dx.doi.org/10.1016/j.molcel.2013.10.021

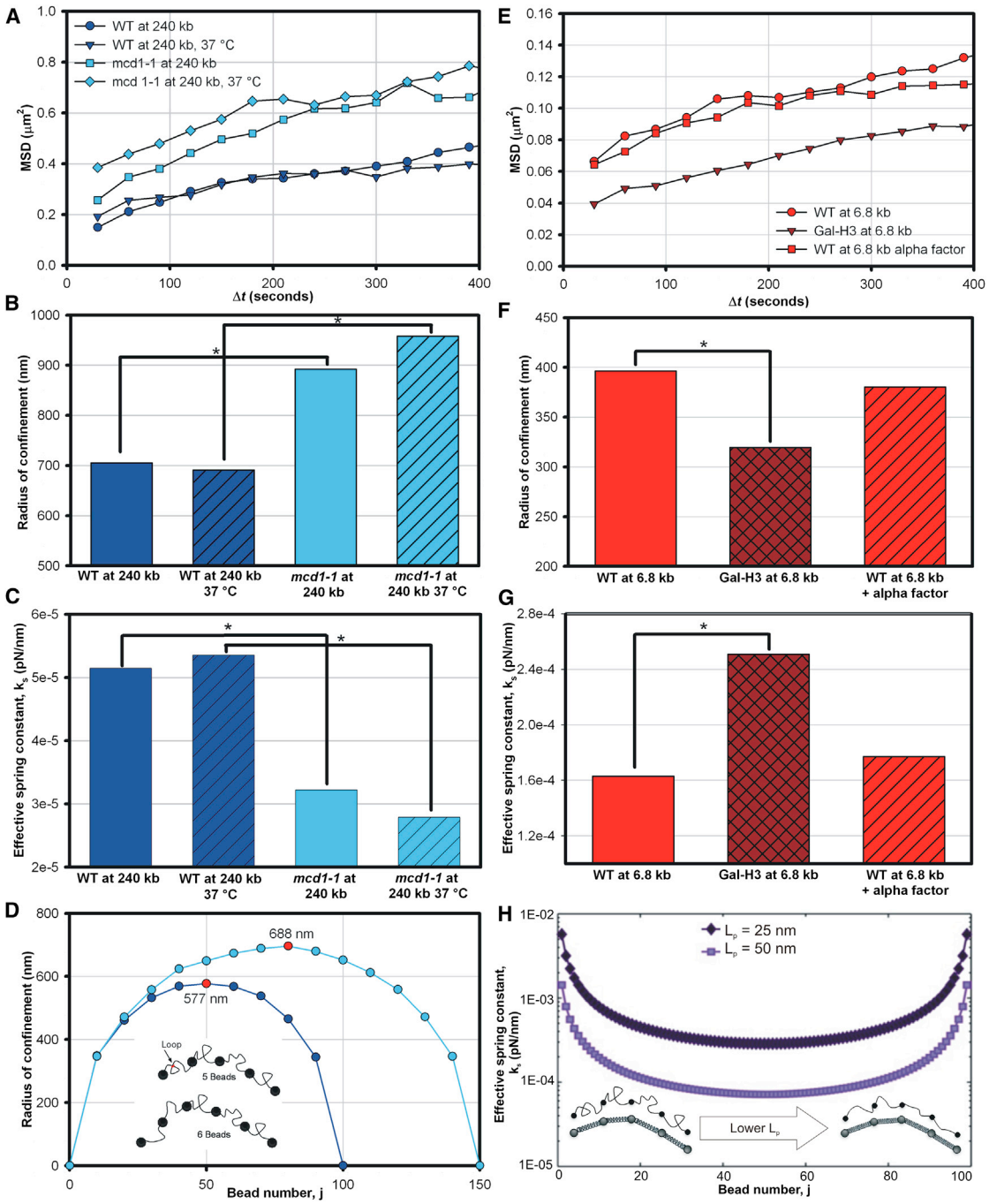

Figure 5. Loss of Cohesin or Nucleosome Depletion during Interphase Results in Altered Confinement and Chromatin Stiffness

(A) Upon depletion of cohesin (*mcd1-1* at 37°C, light blue diamonds), we observed a decrease in confinement of chromatin at 240 kb from the CEN that was not due to the increased temperature (compare to WT at 37°C, dark blue triangles).

(B) Bar graph of R_c values (Equation 2). Statistical comparisons reveal significant increased R_c upon depletion of cohesin in *mcd1-1* cells (Levene's test, $p < 0.05$; Figure S2B).

(C) K_s (Equation 5) is reduced (softened) upon depletion of cohesin as compared to WT at 24°C and 37°C.

(D) We can simulate the effects of depleting cohesin and losing chromatin looping as an increase in the number of beads in our model (inset). This predicts that increasing the number of beads in the chain will result in reduced confinement (688 nm) as compared to the same bead position (middle, red circle) on a shorter chain (577 nm), consistent with experimentally observed data.

(E) MSD curves of lacO/lacI-GFP at 6.8 kb from the CEN in WT, histone-depleted (Gal-H3), and α factor-treated cells.

(legend continued on next page)

Examining Chromosome Territories to Understand Cellular Behaviors like Repair

Our in vivo observations of chromatin fluctuations highlight dynamics and predict significant interactions to allow for a variety of cellular processes (Figure 6). We hypothesize that the organization of chromosomes within the nucleus into territories dictates chromosome interactions. Altering the location of tethering or detaching one chromosome end would allow chromatin to explore a larger volume. These genome-wide changes could be quickly reversed by subsequent reattachment of the chromosomes. The R_c is determined by multiple factors, including tethering, compaction by cohesin, and nucleosomal wrapping (Figures 1D, 2B, 5B, and 6B). Various model systems have shown that the total R_c is similar across species (Chubb and Bickmore, 2003; Gasser, 2002; Soutoglou and Misteli, 2007), suggesting that this may be at least in part dictated by an inherent property of the polymer. Attenuation of these properties could contribute to facilitating chromosome interactions upon damage and form the basis for mechanism of action for a wide range of pathways that serve to increase or decrease chromatin motion, such as DNA repair or gene gating. Based on the increased confinement and stiffening of the chromosome upon reduction of nucleosome occupancy, we hypothesize that attenuation of nucleosomal wrapping could play an important role in dictating the dynamics of DNA repair by reducing L_p. We have previously shown that dynamic exchange of nucleosomes is important for maintenance of the pericentromeric chromatin under tension (Verdaasdonk et al., 2012). The work presented here provides a basic framework for an integrated understanding of physical organization and dynamic interactions dictated by chromatin modifications to explain complex cellular behaviors such as DNA repair.

Changes in the R_c have been observed upon DNA damage, both for damaged and undamaged chromosomes (Dion et al., 2012; Haber and Leung, 1996; Miné-Hattab and Rothstein, 2012). The increased range of motion of a double-stranded break is thought to allow the damaged site to explore a much larger area within the nucleus to promote homology search for repair. The increased motion of damaged chromatin is known to require the recombination proteins Rad51 and Rad54, and the DNA damage response pathway components Mec1 and Rad9 (Dion et al., 2012; Miné-Hattab and Rothstein, 2012). Interestingly, Mec1 checkpoint activity is important to maintain replication fork integrity by detaching tethered and highly transcribed regions from the nuclear pore (Bermejo et al., 2011). This mechanism of detachment cannot explain the increased motion observed upon DNA damage (Ira and Hastings, 2012) but could suggest an alternative role for the DNA damage response pathway in maintaining chromatin tethering. These data highlight the importance of tethering to regulate chromatin motion, and further work should examine which points of tethering are altered upon DNA damage.

EXPERIMENTAL PROCEDURES

For detailed growth and imaging conditions, see Supplemental Experimental Procedures. Strains used are listed in Table S2.

Image Analysis

For MSD analysis, the images were identically analyzed using MetaMorph (Molecular Devices, Sunnyvale) and MATLAB (The Mathworks, Natick). The GFP and RFP foci of the brightest planes per time point were tracked using a custom MATLAB program (Speckle Tracker) as previously described (Wan, 2008; Wan et al., 2009, 2012). These coordinates were further analyzed using MATLAB and Excel (Microsoft, Redmond) software to determine MSD. The RFP coordinates were subtracted from the GFP coordinates to eliminate cell and nuclear motion. We then examined the 2D change in position of the lacO/lacI-GFP chromatin spot over increasing time lags using a classical MSD approach at each time interval,

$$MSD_\tau = \left\langle (x_{t+\tau} - x_t)^2 + (y_{t+\tau} - y_t)^2 \right\rangle, \qquad \text{(Equation 6)}$$

for all time lags τ. Only cells whose MSD curves exhibited a linear slope within the (1.5×IQR) range were included in subsequent analysis. Figures were made using SigmaPlot (Systat Software, San Jose).

To measure spot size, we used a custom GUI written in MATLAB as described previously (Haase et al., 2012). The spot intensity distribution is fit with a 2D Gaussian function, and full width-full maximum values are used to determine spot size.

Calculating R_c from Experimental Data

We calculate R_c from the 2D MSD plateau value as (Neumann et al., 2012)

$$R_c = \frac{5}{4} * \sqrt{MSD_{plateau}}, \qquad \text{(Equation 1)}$$

where the plateau is measured from the 330–390 s region of the time lapse, as most cells have reached confinement at this point while minimizing potential errors introduced by MSD analysis at longer time lags.

We calculate the variance of the distribution of spot positions as $\sigma^2 = mean(\sigma_x^2,\ \sigma_y^2)$ where these are measured using MATLAB to fit the spot positions as $[\mu_x,\ \sigma_x] = normfit(x - x_{mean})$ and $[\mu_y,\ \sigma_y] = normfit(y - y_{mean})$. We then use σ^2 to calculate R_c as

$$R_c = \frac{5}{4} * \sqrt{2\sigma^2 + \langle \Delta r_0^2 \rangle}, \qquad \text{(Equation 2)}$$

where the average squared deviation from the mean position is $\langle \Delta r_0^2 \rangle = \langle \Delta x_0^2 \rangle + \langle \Delta y_0^2 \rangle$.

Entropic Bead-Spring Chain Model

We model chromosomes as chains composed of N+1 beads connected by N linear springs. The equation of motion for a bead i at position X_i is given by Doi and Edwards (1986) as

$$\frac{d\hat{\boldsymbol{X}}_i}{d\hat{t}} = \frac{1}{\zeta}\left(\hat{\boldsymbol{F}}_i^B(t) + \hat{\boldsymbol{F}}_i^S(t) + \hat{\boldsymbol{F}}_i^{EV}(t) + \hat{\boldsymbol{F}}_i^W(t)\right), \qquad \text{(Equation 7)}$$

for $i = 0,\ 1,\ \ldots,\ N+1$. Here ζ is the bead drag coefficient, $\boldsymbol{F}_i^B$ is the Brownian force, $\boldsymbol{F}_i^S$ is the spring force, $\boldsymbol{F}_i^{EV}$ is the excluded volume force, and $\boldsymbol{F}_i^W$ captures the interaction of the bead with the cell walls. In this work we use the following dimensionless variables:

(F and G) (F) R_c is reduced (more confined; Equation 2) and (G) effective k_s is increased (stiffer; Equation 5) upon depletion of histone H3. Statistical comparisons show a significant difference in both R_c and k_s upon histone depletion ($p < 0.05$) and no significant difference upon α factor treatment ($p > 0.05$) (Levene's test, $p < 0.05$; Figure S2C).

(H) We hypothesize that reducing nucleosome density by depleting histone H3 will result in reduced L_p (from chromatin to DNA, [Bloom, 2008]). Our doubly tethered bead-spring model predicts an increase in k_s upon reduction of L_p (from $L_p = 50$ to $L_p = 25$ nm), consistent with experimentally observed increase in k_s at 6.8 kb from the CEN upon nucleosome depletion.

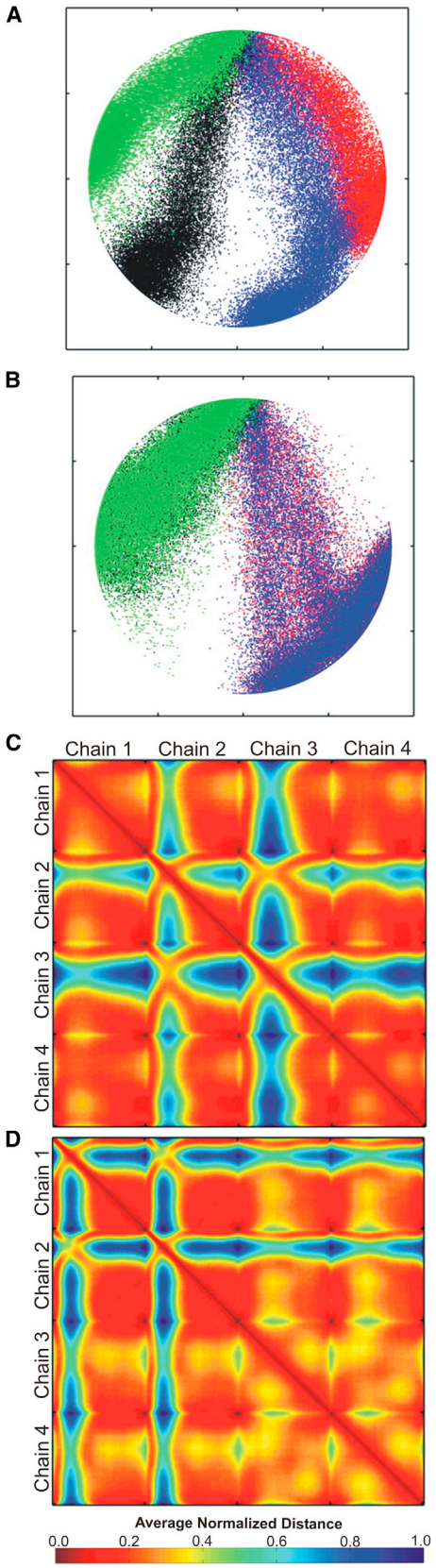

Figure 6. Modeling the Chromatin Spring as a Doubly Tethered, Confined Bead-Spring Chain with Excluded Volume Interactions Can Recapitulate Chromosome Territory Formation as Observed by Chromosome Interaction Heatmaps

We have tracked bead positions over time for a single run for chains in which one end (CEN-SPB attachment) is at the top of the circle (at 0 degrees) and the other end (telomere attachment) is tethered at (A) four discrete positions (equally distributed between 90 and 298 degrees) or (B) tethered at two discrete positions (90 and 298 degrees). Heatmap representation for the average distance during a run between all beads for (C) four discrete attachment points and (D) two attachment points. Heatmap values have been normalized to 1 to account for different maximum distances between model runs. For a value of 0, the beads are separated by a small distance and thus highly likely to come into physical contact, whereas a value of 1 represents a large spatial separation and low probability of contact. Chain 1, red; chain 2, blue; chain 3, black; chain 4, green.

$$\boldsymbol{X}_i = \widehat{\boldsymbol{X}}_i\sqrt{\frac{k_s^0}{k_BT}},\ t = \widehat{t}\,\frac{2k_s^0}{\zeta},\ \boldsymbol{F} = \widehat{\boldsymbol{F}}\,\frac{1}{\sqrt{k_s^0 k_BT}},\ \text{where } k_s^0 = \frac{3k_BT}{(2L_p)^2}. \quad \text{(Equation 8)}$$

- *Brownian Force.* The Brownian force is $\widehat{\boldsymbol{F}}_i^B = \sqrt{2k_BT\zeta}\,\boldsymbol{W}_i$, or in dimensionless form,

$$\boldsymbol{F}_i^B = \boldsymbol{W}_i, \quad \text{(Equation 9)}$$

where $\boldsymbol{W}_i$ is a Wiener process:

$$\langle \boldsymbol{W}_i(t)\rangle = 0,$$

$$\langle \boldsymbol{W}_i(t)\boldsymbol{W}_j(t')\rangle = \delta_{ij}\,\min(t,t').$$

- *Spring Force.* We consider linear springs so that the spring force acting on bead *i* is

$$\boldsymbol{F}_i^S = 2\boldsymbol{X}_i - \boldsymbol{X}_{i-1} - \boldsymbol{X}_{i+1}, \quad \text{(Equation 10)}$$

for $i = 1, 2, \ldots, N$.

- *Excluded Volume Force.* The excluded volume interaction is modeled using a soft potential as in Jendrejack (2002),

$$\boldsymbol{F}_i^{EV} = \frac{z}{4d^5}\left(\sum_{j=0,\,j\neq i}^{N}(\boldsymbol{X}_i - \boldsymbol{X}_j)\exp\left[-\frac{(\boldsymbol{X}_i - \boldsymbol{X}_j)^2}{2d^2}\right]\right). \quad \text{(Equation 11)}$$

Here the dimensionless parameters *z* and *d* are, respectively, measures of the strength and range of the interaction.

- *Wall Interaction.* To model the bead-wall interaction, whenever a bead moves outside the confining circle, it is moved to the nearest point on the boundary before the next time step (Jones et al., 2011).

Effective Spring Constant in a Double-Tethered Rouse Chain

If we consider that the only forces are $\boldsymbol{F}_i^B$ and $\boldsymbol{F}_i^S$, then the model becomes a double-tethered Rouse chain. In this case the effective spring constant for bead *i* can be found explicitly as

$$k_{s,i} = 3k_BT\left(\frac{C_r}{2L_p \times L_c}\right)\left(\frac{1}{p(1-p)}\right), \quad \text{(Equation 3)}$$

where k_B is the Boltzmann constant, T is temperature (Kelvin), L_p is persistence length, L_c is contour length, C_r is ratio of compaction, and p is the percentage

of the chain from the CEN (i.e., for CEN p = 0 and for the telomere p = 1). The first term, $3k_BT$, is the thermal contribution, the second, $(C_r/2L_p \times L_c)$, captures the properties of the chromatin, and the last, $(1/p(1-p))$, measures relative location within the chromatin.

Defining Model Variables

The model requires two parameters: N and L_p. To determine N, we first estimate chromosome length in the cell by dividing the chromosome length in bp (contour length, L_c) by the packing density (ratio of compaction, C_r). For an average chromosome of L_c ~800,000 bp and a packing density is 80 bp/nm (~4× nucleosomal chromatin), then its length in the nucleus is 10,000 nm (L_c/C_r). The packing density is less than the 30 nm fiber (~6× the 11 nm fiber) due to the lack of evidence for the 30 nm fiber and the reduced compaction of yeast chromatin relative to chromosomes in larger cells. The number of beads is derived from the nuclear length divided by the L_p, 10,000 nm/50 nm = 200 beads. Since we model the polymer from the CEN to the telomere, we use N = 100 beads. L_p and packing density vary proportionally and cannot be independently deduced from the model. Simulations of 100 beads with L_p = 50 nm or 25 beads with L_p = 100 nm predict motion plots comparable to that shown in Figure 1A. The modeled R_c using 100 beads and L_p = 50 nm compares closely with literature values (dashed line; Figure 1D). These assigned values are not unique parameters, and it is likely that in vivo conditions include a wide range of values.

Calculating Effective k_s from Experimental Data

Although the motion in vivo is ATP dependent (Figure S5; Weber et al., 2012), it is still random in nature with step sizes following a Gaussian distribution, supporting the assumption that the beads move in a harmonic potential well at some effective temperature (Tokuda et al., 2012). In this manner, it is possible to group the different components of energy-dependent motion in the single nondirectional temperature parameter (T).

To calculate effective k_s from the plateau value of the 2D MSD plot, we consider the equation (Uhlenbeck and Ornstein, 1930)

$$MSD = 2\frac{k_S T}{k_s}\left(1 - e^{-\zeta t/(2k_S)}\right) + 2\left\langle \Delta r_0^2 \right\rangle \left(1 - e^{-\varpi t/(ks)}\right)^2. \quad \text{(Equation 12)}$$

This means that when t is very large, the plateau value is

$$MSD_{\text{plateau}} = 2\frac{k_B T}{k_s} + \left\langle \Delta r_0^2 \right\rangle, \quad \text{(Equation 13)}$$

where the average squared deviation from the mean position is

$$\left\langle \Delta r_0^2 \right\rangle = \left\langle \Delta x_0^2 \right\rangle + \left\langle \Delta y_0^2 \right\rangle. \quad \text{(Equation 14)}$$

Solving Equation 13 gives the spring constant as

$$k_s = \frac{2k_B T}{MSD_{\text{plateau}} - \left\langle \Delta r_0^2 \right\rangle}. \quad \text{(Equation 4)}$$

To illustrate how to calculate effective k_s from variance of lacO spot position, we look at the simplest case: a bead moving by Brownian motion and attached to a fixed point by a linear spring. The bead position obeys the following Lagevin equation:

$$\zeta d\mathbf{X} = -k_s \mathbf{X} dt + \sqrt{2k_B T \zeta} d\mathbf{W}, \quad \text{(Equation 15)}$$

where, as before, **W** is a Wiener process.

Equation 15 has a corresponding Fokker-Planck equation with solution

$$P(\boldsymbol{X}) = \sim \exp\left(-\frac{k_s}{k_B T}\frac{\boldsymbol{X}^2}{2}\right). \quad \text{(Equation 16)}$$

This means that a histogram of the distribution of bead positions has a Gaussian form with variance $\sigma^2 = k_B T/k_s$. Then from the variance of the distribution, one can obtain the spring constant as

$$k_s = \frac{k_B T}{\sigma^2}. \quad \text{(Equation 5)}$$

Statistical Analysis

We used the equipartition Equations 2 and 5 and the standard deviation from the whole population of cells for remaining comparisons. This results in a single value from the whole population standard deviation (with no associated error bars), and for statistical comparison we compare the homogeneity of population variances by Levene's test (Figure S2; Levene, 1960). For additional details, see Supplemental Information and Figure S1.

SUPPLEMENTAL INFORMATION

Supplemental Information includes six figures, two tables, and Supplemental Experimental Procedures and can be found with this article online at http://dx.doi.org/10.1016/j.molcel.2013.10.021.

ACKNOWLEDGMENTS

We thank members of the Bloom laboratory for discussion, advice, and critical readings of the manuscript. This work was funded by the National Institutes of Health R37 grant GM32238 (to K.B.) and the National Science Foundation grants DMS-1100281 and DMR-1122483 (to M.G.F.).

Received: May 28, 2013
Revised: September 10, 2013
Accepted: October 14, 2013
Published: November 21, 2013

REFERENCES

Albert, B., Léger-Silvestre, I., Normand, C., and Gadal, O. (2012). Nuclear organization and chromatin dynamics in yeast: biophysical models or biologically driven interactions? Biochim. Biophys. Acta *1819*, 468–481.

Austin, C.M., and Bellini, M. (2010). The dynamic landscape of the cell nucleus. Mol. Reprod. Dev. *77*, 19–28.

Berger, A.B., Cabal, G.G., Fabre, E., Duong, T., Buc, H., Nehrbass, U., Olivo-Marin, J.C., Gadal, O., and Zimmer, C. (2008). High-resolution statistical mapping reveals gene territories in live yeast. Nat. Methods *5*, 1031–1037.

Bermejo, R., Capra, T., Jossen, R., Colosio, A., Frattini, C., Carotenuto, W., Cocito, A., Doksani, Y., Klein, H., Gómez-González, B., et al. (2011). The replication checkpoint protects fork stability by releasing transcribed genes from nuclear pores. Cell *146*, 233–246.

Bickmore, W.A., and van Steensel, B. (2013). Genome architecture: domain organization of interphase chromosomes. Cell *152*, 1270–1284.

Bloom, K.S. (2008). Beyond the code: the mechanical properties of DNA as they relate to mitosis. Chromosoma *117*, 103–110.

Bouck, D.C., and Bloom, K. (2007). Pericentric chromatin is an elastic component of the mitotic spindle. Curr. Biol. *17*, 741–748.

Boveri, T. (1909). Die Blastomerenkerne von *Ascaris megalocephala* und die Theorie der Chromosomenindividualität. Arch. Zellforsch. *3*, 181–268.

Brickner, D.G., Cajigas, I., Fondufe-Mittendorf, Y., Ahmed, S., Lee, P.C., Widom, J., and Brickner, J.H. (2007). H2A.Z-mediated localization of genes at the nuclear periphery confers epigenetic memory of previous transcriptional state. PLoS Biol. *5*, e81.

Bruno, L., Salierno, M., Wetzler, D.E., Despósito, M.A., and Levi, V. (2011). Mechanical properties of organelles driven by microtubule-dependent molecular motors in living cells. PLoS ONE *6*, e18332.

Bystricky, K., Heun, P., Gehlen, L., Langowski, J., and Gasser, S.M. (2004). Long-range compaction and flexibility of interphase chromatin in budding

yeast analyzed by high-resolution imaging techniques. Proc. Natl. Acad. Sci. USA *101*, 16495–16500.

Bystricky, K., Laroche, T., van Houwe, G., Blaszczyk, M., and Gasser, S.M. (2005). Chromosome looping in yeast: telomere pairing and coordinated movement reflect anchoring efficiency and territorial organization. J. Cell Biol. *168*, 375–387.

Chubb, J.R., and Bickmore, W.A. (2003). Considering nuclear compartmentalization in the light of nuclear dynamics. Cell *112*, 403–406.

Cook, P.R., and Marenduzzo, D. (2009). Entropic organization of interphase chromosomes. J. Cell Biol. *186*, 825–834.

Cremer, T., and Cremer, M. (2010). Chromosome territories. Cold Spring Harb. Perspect. Biol. *2*, a003889.

Dekker, J., Rippe, K., Dekker, M., and Kleckner, N. (2002). Capturing chromosome conformation. Science *295*, 1306–1311.

de Wit, E., and de Laat, W. (2012). A decade of 3C technologies: insights into nuclear organization. Genes Dev. *26*, 11–24.

Dion, V., Kalck, V., Horigome, C., Towbin, B.D., and Gasser, S.M. (2012). Increased mobility of double-strand breaks requires Mec1, Rad9 and the homologous recombination machinery. Nat. Cell Biol. *14*, 502–509.

Dixon, J.R., Selvaraj, S., Yue, F., Kim, A., Li, Y., Shen, Y., Hu, M., Liu, J.S., and Ren, B. (2012). Topological domains in mammalian genomes identified by analysis of chromatin interactions. Nature *485*, 376–380.

Doi, M., and Edwards, S.F. (1986). The Theory of Polymer Dynamics. (Oxford: Oxford University Press).

Drubin, D.A., Garakani, A.M., and Silver, P.A. (2006). Motion as a phenotype: the use of live-cell imaging and machine visual screening to characterize transcription-dependent chromosome dynamics. BMC Cell Biol. *7*, 19.

Duan, Z., Andronescu, M., Schutz, K., McIlwain, S., Kim, Y.J., Lee, C., Shendure, J., Fields, S., Blau, C.A., and Noble, W.S. (2010). A three-dimensional model of the yeast genome. Nature *465*, 363–367.

Finan, K., Cook, P.R., and Marenduzzo, D. (2011). Non-specific (entropic) forces as major determinants of the structure of mammalian chromosomes. Chromosome Res. *19*, 53–61.

Gasser, S.M. (2002). Visualizing chromatin dynamics in interphase nuclei. Science *296*, 1412–1416.

Haase, J., Stephens, A., Verdaasdonk, J., Yeh, E., and Bloom, K. (2012). Bub1 kinase and Sgo1 modulate pericentric chromatin in response to altered microtubule dynamics. Curr. Biol. *22*, 471–481.

Haber, J.E., and Leung, W.Y. (1996). Lack of chromosome territoriality in yeast: promiscuous rejoining of broken chromosome ends. Proc. Natl. Acad. Sci. USA *93*, 13949–13954.

Haering, C.H., and Jessberger, R. (2012). Cohesin in determining chromosome architecture. Exp. Cell Res. *318*, 1386–1393.

Hediger, F., Neumann, F.R., Van Houwe, G., Dubrana, K., and Gasser, S.M. (2002). Live imaging of telomeres: yKu and Sir proteins define redundant telomere-anchoring pathways in yeast. Curr. Biol. *12*, 2076–2089.

Heun, P., Laroche, T., Shimada, K., Furrer, P., and Gasser, S.M. (2001). Chromosome dynamics in the yeast interphase nucleus. Science *294*, 2181–2186.

Hill, A., and Bloom, K. (1987). Genetic manipulation of centromere function. Mol. Cell. Biol. *7*, 2397–2405.

Hübner, M.R., and Spector, D.L. (2010). Chromatin dynamics. Annu. Rev. Biophys. *39*, 471–489.

Ira, G., and Hastings, P.J. (2012). DNA breakage drives nuclear search. Nat. Cell Biol. *14*, 448–450.

Jendrejack, R.M. (2002). Stochastic simulations of DNA in flow: dynamics and the effects of hydrodynamic interactions. J. Chem. Phys. *116*, 7752.

Jin, Q.W., Fuchs, J., and Loidl, J. (2000). Centromere clustering is a major determinant of yeast interphase nuclear organization. J. Cell Sci. *113*, 1903–1912.

Jones, J.J., van der Maarel, J.R., and Doyle, P.S. (2011). Effect of nanochannel geometry on DNA structure in the presence of macromolecular crowding agent. Nano Lett. *11*, 5047–5053.

Kamiti, M., and van de Ven, T.G.M. (1996). Measurement of spring constants of polyacrylamide chains bridging particles to a solid surface. Macromolecules *29*, 1191–1194.

Levene, H. (1960). Robust tests for quality of variances. In Contribution to Probability and Statistics: Essays in Honour of Harold Hotelling, I. Olkin, ed. (Stanford, NJ: Stanford University Press), pp. 278–292.

Miné-Hattab, J., and Rothstein, R. (2012). Increased chromosome mobility facilitates homology search during recombination. Nat. Cell Biol. *14*, 510–517.

Neumann, F.R., Dion, V., Gehlen, L.R., Tsai-Pflugfelder, M., Schmid, R., Taddei, A., and Gasser, S.M. (2012). Targeted INO80 enhances subnuclear chromatin movement and ectopic homologous recombination. Genes Dev. *26*, 369–383.

O'Toole, E.T., Winey, M., and McIntosh, J.R. (1999). High-voltage electron tomography of spindle pole bodies and early mitotic spindles in the yeast Saccharomyces cerevisiae. Mol. Biol. Cell *10*, 2017–2031.

Rabl, C. (1885). Über Zelltheilung. Morph. Jb. *10*, 214–330.

Rosa, A., and Everaers, R. (2008). Structure and dynamics of interphase chromosomes. PLoS Comput. Biol. *4*, e1000153.

Sanyal, A., Baù, D., Martí-Renom, M.A., and Dekker, J. (2011). Chromatin globules: a common motif of higher order chromosome structure? Curr. Opin. Cell Biol. *23*, 325–331.

Scheffold, F., Díaz-Leyva, P., Reufer, M., Ben Braham, N., Lynch, I., and Harden, J.L. (2010). Brushlike interactions between thermoresponsive microgel particles. Phys. Rev. Lett. *104*, 128304.

Schober, H., Kalck, V., Vega-Palas, M.A., Van Houwe, G., Sage, D., Unser, M., Gartenberg, M.R., and Gasser, S.M. (2008). Controlled exchange of chromosomal arms reveals principles driving telomere interactions in yeast. Genome Res. *18*, 261–271.

Seitan, V.C., and Merkenschlager, M. (2012). Cohesin and chromatin organisation. Curr. Opin. Genet. Dev. *22*, 93–100.

Sofueva, S., and Hadjur, S. (2012). Cohesin-mediated chromatin interactions—into the third dimension of gene regulation. Brief Funct. Genomics *11*, 205–216.

Soutoglou, E., and Misteli, T. (2007). Mobility and immobility of chromatin in transcription and genome stability. Curr. Opin. Genet. Dev. *17*, 435–442.

Spector, D.L. (2003). The dynamics of chromosome organization and gene regulation. Annu. Rev. Biochem. *72*, 573–608.

Stephens, A.D., Haase, J., Vicci, L., Taylor, R.M., 2nd, and Bloom, K. (2011). Cohesin, condensin, and the intramolecular centromere loop together generate the mitotic chromatin spring. J. Cell Biol. *193*, 1167–1180.

Stephens, A.D., Haggerty, R.A., Vasquez, P.A., Vicci, L., Snider, C.E., Shi, F., Quammen, C., Mullins, C., Haase, J., Taylor, R.M., 2nd., et al. (2013). Pericentric chromatin loops function as a nonlinear spring in mitotic force balance. J. Cell Biol. *200*, 757–772.

Taddei, A., and Gasser, S.M. (2012). Structure and function in the budding yeast nucleus. Genetics *192*, 107–129.

Taddei, A., Schober, H., and Gasser, S.M. (2010). The budding yeast nucleus. Cold Spring Harb. Perspect. Biol. *2*, a000612.

Tjong, H., Gong, K., Chen, L., and Alber, F. (2012). Physical tethering and volume exclusion determine higher-order genome organization in budding yeast. Genome Res. *22*, 1295–1305.

Tokuda, N., Terada, T.P., and Sasai, M. (2012). Dynamical modeling of three-dimensional genome organization in interphase budding yeast. Biophys. J. *102*, 296–304.

Uhlenbeck, G.E., and Ornstein, L.S. (1930). On the Theory of the Brownian Motion. Phys. Rev. *36*, 823–841.

Verdaasdonk, J.S., Gardner, R., Stephens, A.D., Yeh, E., and Bloom, K. (2012). Tension-dependent nucleosome remodeling at the pericentromere in yeast. Mol. Biol. Cell *23*, 2560–2570.

Wan, X. (2008). Asymmetric chromosome oscillation during mitosis and protein architecture of the human kinetochore measured by K-SHREC Kinetochore-Speckle High Resolution Co-Localization. PhD thesis, University of North Carolina at Chapel Hill, Chapel Hill, NC. http://dc.lib.unc.edu/cdm/ref/collection/etd/id/2050.

Wan, X., O'Quinn, R.P., Pierce, H.L., Joglekar, A.P., Gall, W.E., DeLuca, J.G., Carroll, C.W., Liu, S.T., Yen, T.J., McEwen, B.F., et al. (2009). Protein architecture of the human kinetochore microtubule attachment site. Cell *137*, 672–684.

Wan, X., Cimini, D., Cameron, L.A., and Salmon, E.D. (2012). The coupling between sister kinetochore directional instability and oscillations in centromere stretch in metaphase PtK1 cells. Mol. Biol. Cell *23*, 1035–1046.

Weber, S.C., Spakowitz, A.J., and Theriot, J.A. (2012). Nonthermal ATP-dependent fluctuations contribute to the in vivo motion of chromosomal loci. Proc. Natl. Acad. Sci. USA *109*, 7338–7343.

Wong, H., Marie-Nelly, H., Herbert, S., Carrivain, P., Blanc, H., Koszul, R., Fabre, E., and Zimmer, C. (2012). A predictive computational model of the dynamic 3D interphase yeast nucleus. Curr. Biol. *22*, 1881–1890.

Zimmer, C., and Fabre, E. (2011). Principles of chromosomal organization: lessons from yeast. J. Cell Biol. *192*, 723–733.